

Article

Overall and Local Wind Loads on Post-Installed Elevator Shaft of Existing Buildings

Haowen You ¹, Chenxu Si ^{2,*}, Xinwen Ma ^{1,3} and Jingmiao Shang ²

¹ Guangdong Institute of Special Equipment Inspection and Research, Huizhou Inspection Institute, Huizhou 516003, China; youhaowen@hztj.onexmail.com (H.Y.); 10xwma@stu.edu.cn (X.M.)

² School of Civil Engineering and Architecture, Southwest University of Science and Technology, Mianyang 621010, China; mervin@swust.edu.cn

³ College of Engineering, Shantou University, Shantou 515203, China

* Correspondence: scx@mails.swust.edu.cn; Tel.: +86-132-8123-9542

Abstract: The glass curtain walls of post-installed elevator shafts in existing buildings can be damaged by local wind loads, and the serviceability of an elevator may be affected by excessive overall wind loads, especially in hurricane-prone areas. The overall and local wind load characteristics of elevator shafts with different arrangements (E-type, H-type, I-type) were studied using wind tunnel tests and computational fluid dynamics (CFD) numerical simulations. Firstly, high-frequency base balance wind tunnel tests of these elevator shafts with three arrangements were carried out to obtain the overall wind loads on the elevator shafts. Secondly, a CFD simulation was performed on the post-installed elevator shafts with three arrangements, obtaining the surface local wind pressure distribution of the elevator shafts under different wind directions. Finally, the wind-induced displacement responses of post-installed elevator shafts were analyzed. The results show that the aerodynamic interference of different elevator arrangements (E-type, H-type, I-type) and wind directions have significant effects on the overall local wind loads and wind-induced responses of the post-installed elevator, while the local wind loads on the area of the elevator door are less influenced by the elevator arrangement type than local wind loads on the surface and the overall wind loads of the elevator shafts. The results and conclusions may be helpful for developing the wind-resistant design of a post-installed elevator shaft.



Citation: You, H.; Si, C.; Ma, X.; Shang, J. Overall and Local Wind Loads on Post-Installed Elevator Shaft of Existing Buildings. *Buildings* **2024**, *14*, 110. <https://doi.org/10.3390/buildings14010110>

Academic Editors: Flavio Stochino and Lei Zhao

Received: 10 November 2023

Revised: 14 December 2023

Accepted: 21 December 2023

Published: 31 December 2023



Copyright: © 2023 by the authors. Licensee MDPI, Basel, Switzerland. This article is an open access article distributed under the terms and conditions of the Creative Commons Attribution (CC BY) license (<https://creativecommons.org/licenses/by/4.0/>).

Keywords: wind loads; post-installed elevator shaft; existing buildings; wind tunnel tests

1. Introduction

Due to economic constraints and technical limitations, prior to the 1980s, low- to middle-rise apartment buildings in China were usually built without elevators. However, following rapid socioeconomic development and the trend of an aging population, buildings without elevators are becoming inconvenient, especially for elderly residents [1]. In order to solve this problem, many countries have integrated terms related to the installation of elevator shafts in old apartments into design codes to meet the needs of the elderly, and public opinion has also been taken into account [2,3]. As early as 2007, the Ministry of Housing and Urban–Rural Development in China incorporated the installation of elevators as part of the renovation of old residential areas [4]. In 2018, the work report of the State Council Municipal Government explicitly encouraged the installation of elevators in existing houses for the first time, reflecting the great importance of this livelihood project [5]. German regulations stipulate that elevators must be provided in buildings with five or more residential floors [6].

With increasing numbers of elevator shafts being installed in existing buildings (Figure 1 shows a case of elevator post-installation), many experts and scholars started to investigate the installation arrangement and mechanical performance of post-installed elevator shafts in existing buildings. Ogawa et al. [7,8] proposed alternative schemes of adding elevator shafts to

a staircase, modifying elevator shafts by removing existing stairs, and analyzed the feasibility of implementing the relevant schemes. Niedostatkiewicz et al. [9] investigated the problem of the increase in the width of the expansion joints between an external lift shaft and an existing clinic building and provided a solution by strengthening the soil under the foundation slab of the elevator shaft and reducing the level of groundwater. Chen et al. [10] analyzed the seismic response of a frame structure before and after installing an elevator shaft and concluded that the installed elevator shaft had little influence on the seismic performance of the structure and had a slightly lower seismic response. Marinkovic et al. [11] investigated the degree of damage in buildings after earthquakes and found that masonry infill walls, which were used in some elevator shaft areas instead of reinforced concrete shear walls, led to the insufficient seismic performance of the structures. Some studies on post-installed concrete anchors [12] and the seismic analysis of existing reinforced buildings [13] provide a reference for the mechanical performance analysis of the post-installed elevator shafts of existing buildings. Zhou et al. [14] studied the seismic performance of a light wood structure and found that the use of a masonry elevator shaft in a light wood structure can significantly reduce the displacement at the top of the structure and improve seismic performance. Jiang et al. [15] constructed a set of scale models of multistory masonry structures and carried out a shaking table comparison test. The results show that adding a shear wall elevator shaft in a masonry structure can significantly enhance the lateral seismic performance of the structure.



Figure 1. The case of an installed elevator.

However, the majority of previous research has only focused on specific installation arrangements and the seismic performance of post-installed elevator shafts. As shown in Figure 1, an elevator shaft is usually installed outside a building, and thus is greatly affected by wind loads. When the elevator shaft is subjected to strong winds, the door of the elevator does not close normally, and the glass curtain wall may also be damaged by local wind pressure (as shown in Figure 2). Additionally, the excessive wind-induced responses induced by overall wind loads may affect the serviceability of the elevator. Hence, overall and local wind loads affect the normal and safe operation of the elevator. The distribution characteristics of local surface wind pressure, the overall wind loads, and the dynamic response of wind-induced vibration in post-installed elevator shafts need

to be investigated in detail. Thus far, the wind loads [16–18], aerodynamic interference effects [19–23], and wind-induced responses [24–27] of super high-rise buildings have been widely studied using wind tunnel tests, CFD simulation, and field measurements, which may provide a useful guide to this research. Kim et al. [28], You et al. [29], and Kim and Kanda [30] studied the wind pressure distribution on the surface of high-rise buildings with different taper elevations and step retraction elevations by wind tunnel tests. Mara and Case [31] investigated the effects of corner cuts on the local and overall wind loads of a high-rise building under different wind directions. Tamura et al. [32] studied wind loads on the surface of tall square buildings with spiral elevation. The effects of aerodynamic interference between buildings can result in different wind loads compared with isolated buildings. These aerodynamic interference effects on high-rise buildings have been studied since the 1980s and 1990s [20,33,34]. Xie and Gu [35] and Gu et al. [36] studied the interference effects between two and three buildings with different widths and heights using wind tunnel tests. The influence of the height and breadth ratios of different buildings on aerodynamic interference effects has been investigated in depth [37–41], and the conclusions show that the aerodynamic interference effects were greatly influenced by the height ratios and relative locations between buildings. Moreover, overall wind loads on high-rise buildings have been thoroughly investigated using high-frequency base balance wind tunnel tests. The technique of high-frequency base balance, employed since the early 1980s [26], is the most common method to measure overall wind loads on high-rise buildings. Zhang et al. [42] employed a high-frequency force balance wind tunnel test to investigate overall wind loads on tall square buildings with corner recession. Quan et al. [43] measured overall wind loads on 15 high-rise buildings in four different terrain exposures using high-frequency base balance in wind tunnels. The aerodynamic spectra and base force coefficients of high-rise buildings with different chamfering and recession rates were investigated, and it is concluded that a modification ratio of around 10% decreased the amplitude of the aerodynamic spectrum in most frequency ranges. Tse et al. [44] optimized the wind loads on high-rise buildings via high-frequency base balance tests and concluded that the recession along the height of high-rise buildings has a better effect on reducing the along-wind and cross-wind loads than the chamfer method.



Figure 2. Damage to a glass curtain wall around the installed elevator shaft [45].

To the best of the authors' knowledge, local and overall wind loads on the post-installed elevator shafts have not been investigated in previous studies. To fill this research gap, we studied the overall and local wind loads on post-installed elevator shafts with different arrangements (E-type, H-type, and I-type; as shown in Figure 3) under strong winds. Firstly, the high-frequency base balance wind tunnel tests and numerical simulations based on CFD were introduced. Furthermore, based on the aerodynamic forces measured

using the wind tunnel tests and the wind pressure distribution on the building surface calculated using the CFD model, the aerodynamic coefficients of overall wind loads and the distribution of wind pressure on the surface of post-installed elevator shafts under different wind directions were analyzed. Subsequently, the wind-induced displacement responses were calculated based on the results of wind tunnel tests and the dynamic characteristics extracted from a finite element model of the elevator shafts.

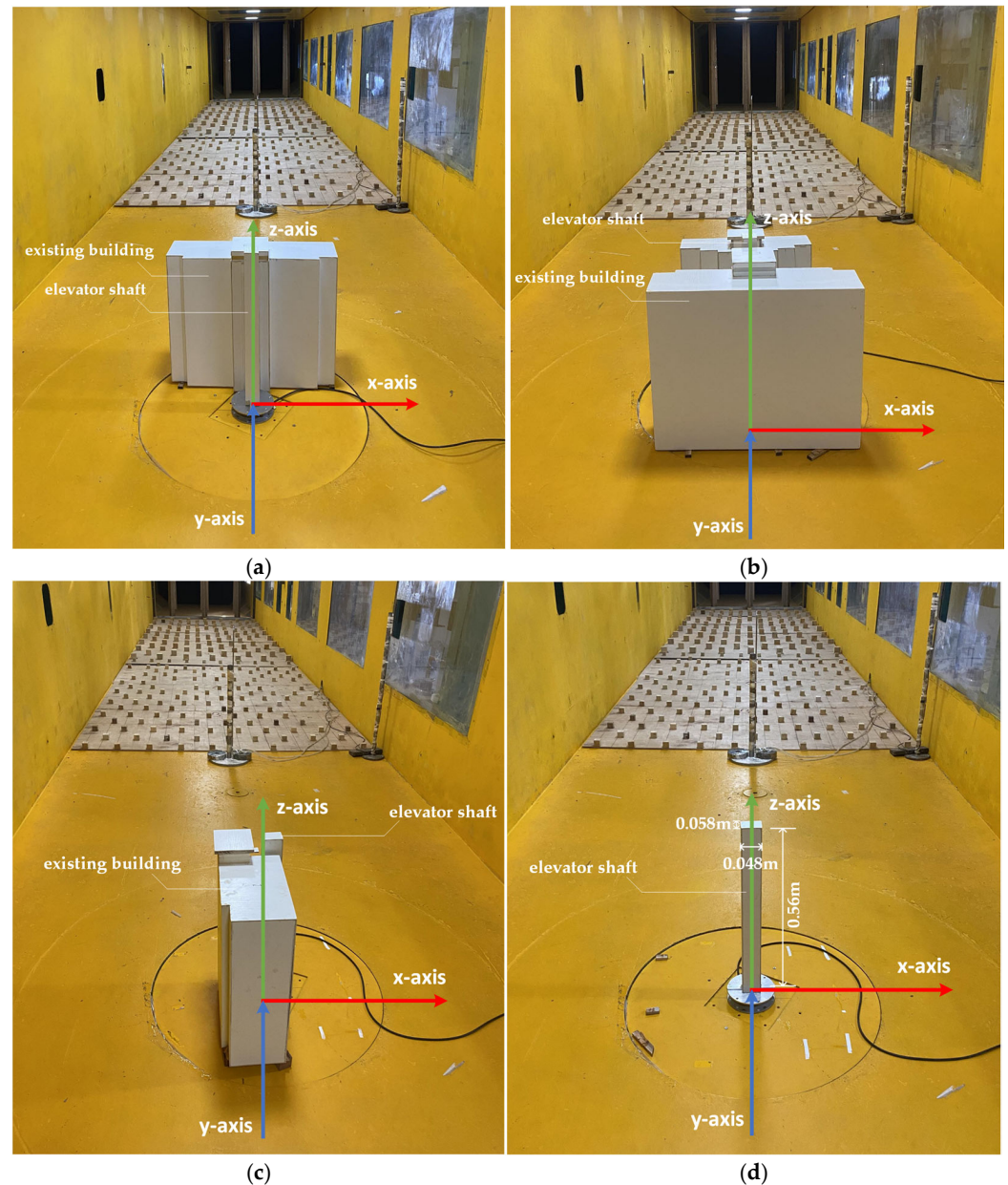


Figure 3. Photos of high-frequency base balance wind tunnel tests on elevator shafts with (a) E-type, (b) H-type, (c) I-type, and (d) S-type arrangements.

2. Local Wind Loads on Post-Installed Elevator Shafts

2.1. CFD Simulation

The CFD simulation was performed with ANSYS Fluent to obtain the local wind loads on the post-installed elevator shafts. The ICEM (The Integrated Computer Engineering and Manufacturing code for Computational Fluid Dynamics) tool was used for pre-processing. The procedural sequence includes constructing a geometric model, planning a computational domain, mesh division, and defining boundary conditions. Subsequently, the ANSYS Fluent version 22.1.0 was employed for mesh validation, solver and turbulence model selec-

tion, material property and boundary condition specification, flow field initialization, and the solving process. Post-processing was conducted using Tecplot version 2021.1.0.113954 to acquire comprehensive wind pressure distributions across diverse arrangements. The definition of wind direction is shown in Figure 4, and the four surfaces of the elevator shafts are marked as No. 1, No. 2, No. 3, and No. 4, respectively. As shown in Figure 5a, the computational domain size is $28H_C$ (flow direction) \times $10H_C$ (span direction) \times $7H_C$ (vertical direction), where H_C is the height of the building center. Unstructured grids were used around the building, structured grids were used in other areas, and grids on the walls of the building and the ground were encrypted, as shown in Figure 5b.

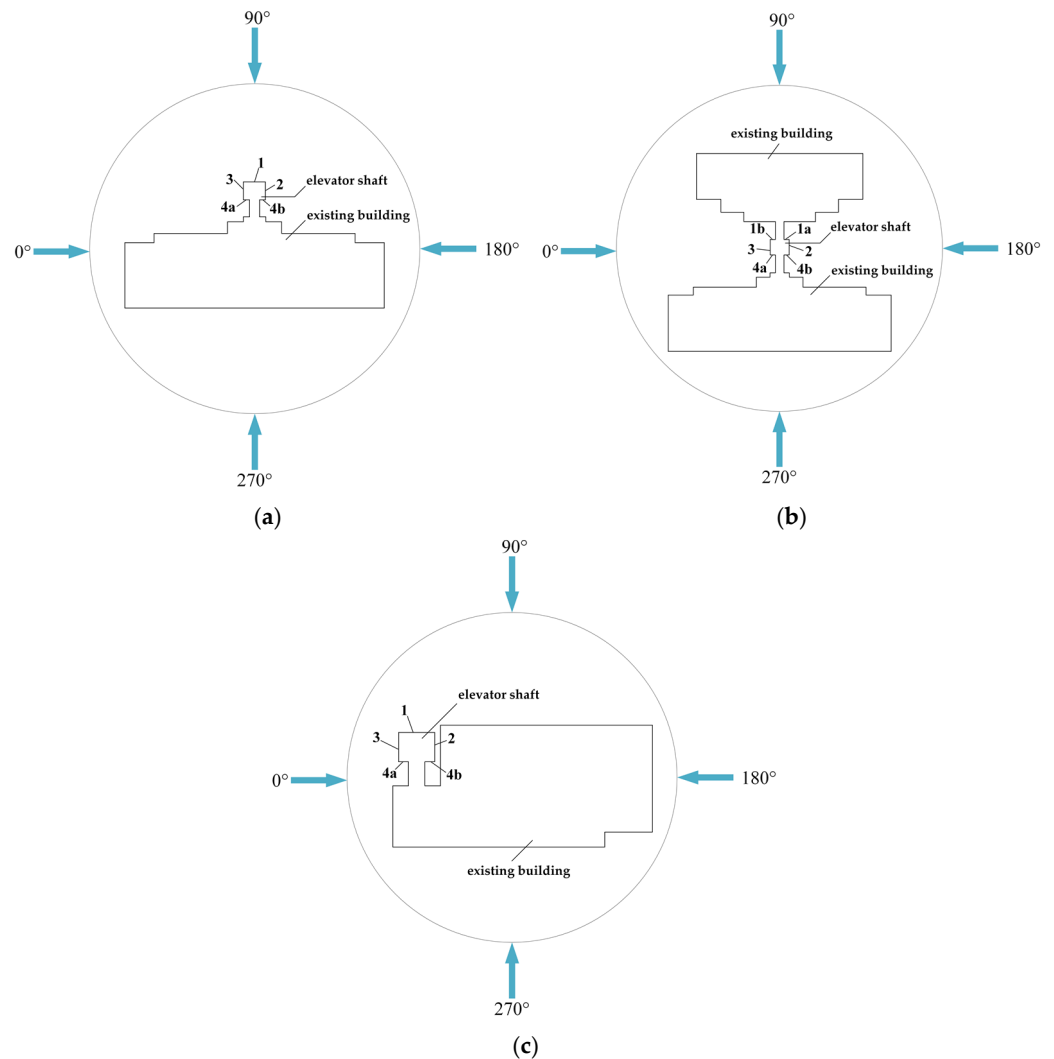


Figure 4. Definition of wind direction and surfaces in CFD simulation: (a) E-type, (b) H-type, and (c) I-type.

The turbulence model adopts an SST κ - ω (2eqn) model, and the pressure–velocity coupling adopts a coupled algorithm. The discrete format of the control equation is second-order upwind format, and the residual convergence standard is 1×10^{-6} .

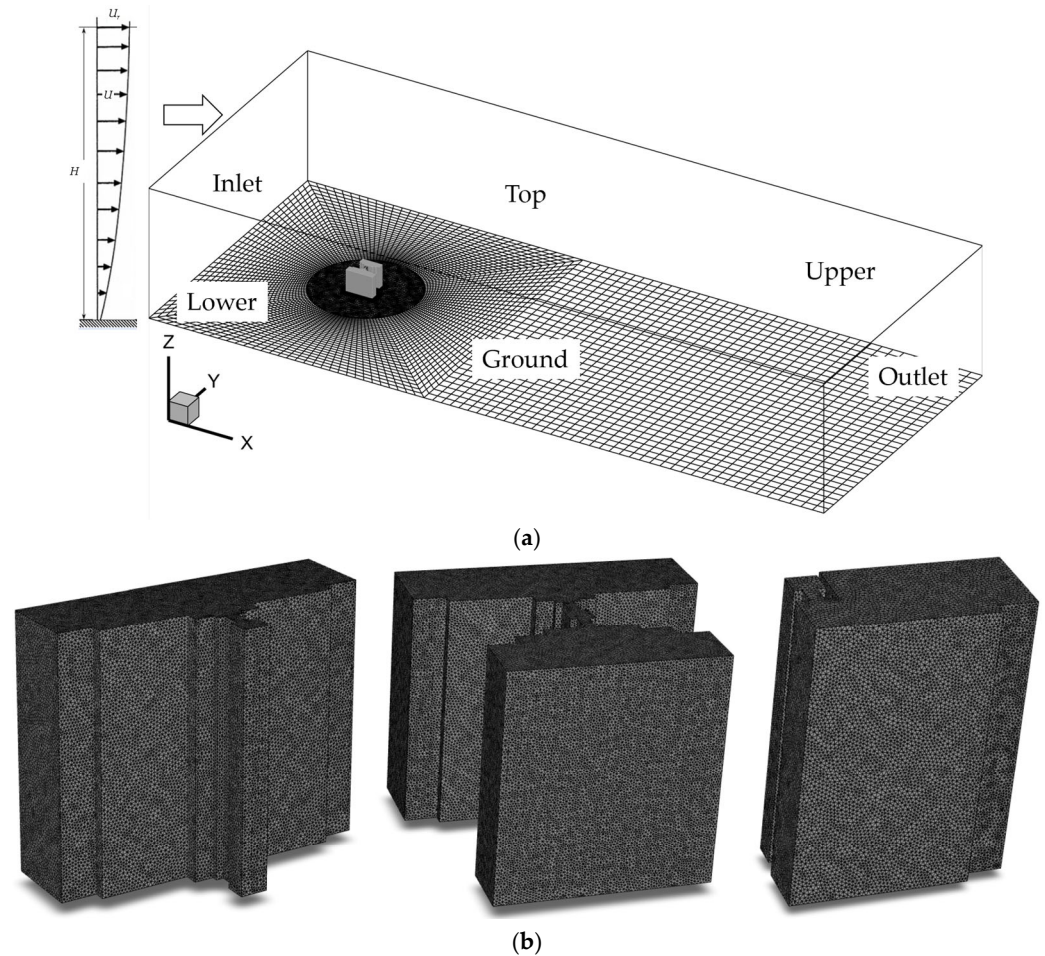


Figure 5. CFD model: (a) computational domain; (b) mesh near the model.

2.2. Results of Local Wind Pressure on Post-Installed Elevator Shaft

The wind pressure on the elevator shafts surface obtained using a CFD simulation can be converted into dimensionless pressure coefficient C_p following:

$$C_p = \frac{P}{\frac{1}{2}\rho v^2} \quad (1)$$

In Equation (1), P , ρ and v are the wind pressure levels acting on the building surface, which can be obtained using simulations of CFD, air density, and reference wind speed, respectively.

The maximum positive and negative wind pressures are essential for the wind-resistant design of an envelope for the post-installed elevator shafts, i.e., an engineer may select the material strength of glass curtain walls and the method of connection between glass curtain walls and structures of a post-installed elevator according to these wind pressures. Figure 6 illustrates the maximum positive and negative coefficients of pressure C_p observed on the four facades of the elevator (shown in Figure 4). With respect to the E-type arrangement, the maximum positive pressure coefficient is 1.12, which occurs in a wind direction of 120° for the No. 2 surface, whereas the maximum negative pressure coefficient is -1.43 , which takes place in a wind direction of 45° for the No. 1 surface. For the H-type arrangement, the maximum positive pressure coefficient is 1.10, which is observed as a wind direction of 120° for the No. 4b surface, while the maximum negative pressure coefficient is -1.11 , which is a wind direction of 135° for the No. 3 surface. For the I-type arrangement, the maximum positive pressure coefficient is 1.14, recorded at a wind direction of 0° for the No. 4a surface, and the maximum negative pressure coefficient is -1.35 , which is observed

as a wind direction of 75° for the No. 2 surface. Among the three arrangement types of the post-installed elevator shafts, both E-type and I-type arrangements exhibit significantly higher levels of maximum positive and negative pressure distributions compared to the H-type arrangement.

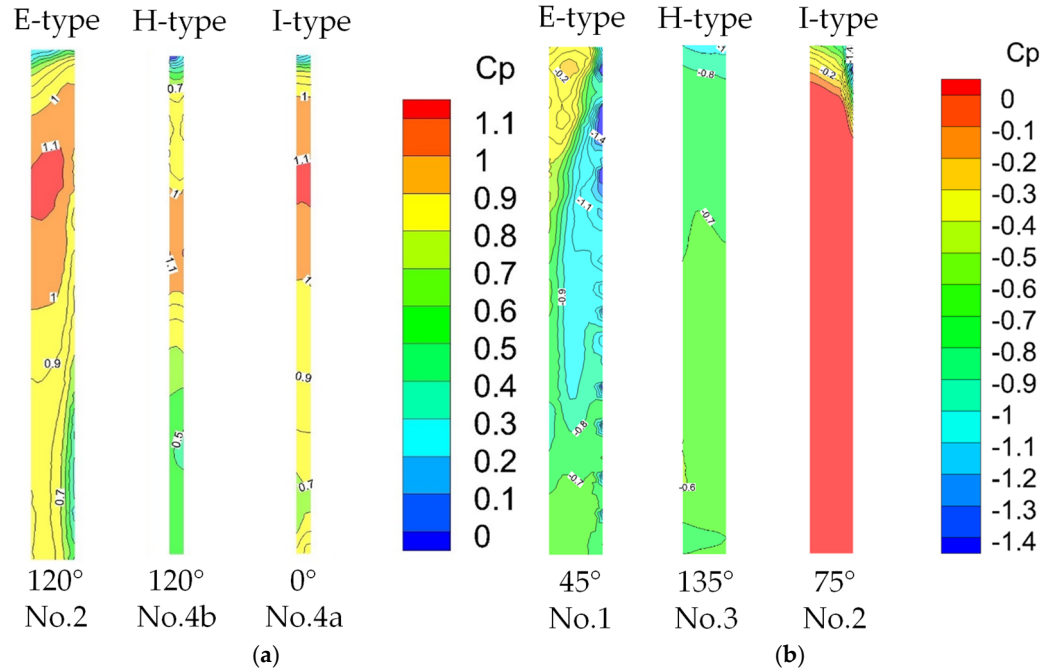


Figure 6. Wind pressure distribution on the surface: (a) maximum positive surface; (b) maximum negative surface.

To study the influences of local wind loads on the functioning of the elevator door, we focused on the area in the middle of the elevator door to investigate variations in mean pressure levels for different wind directions, as shown in Figure 7.

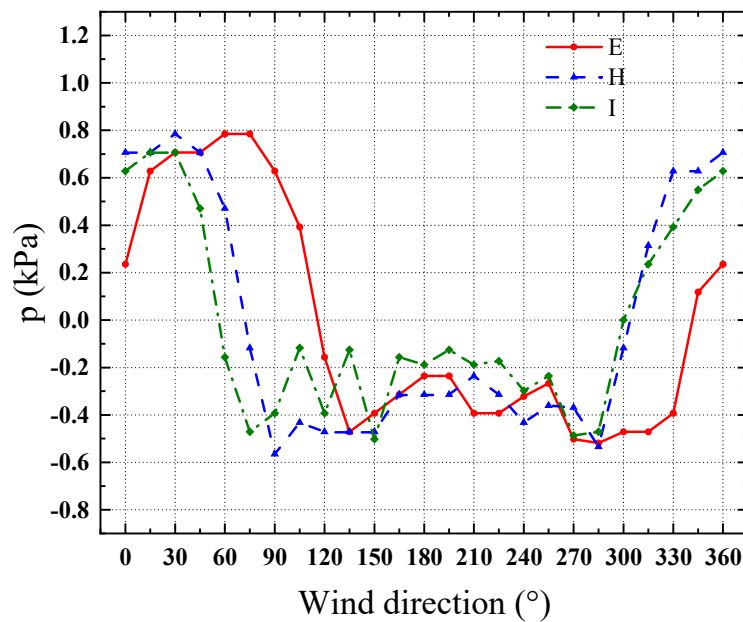


Figure 7. Pressure variation in the middle of the elevator door for different wind directions.

Figure 7 indicates that the general variation in local pressure on the elevator door for different wind directions has a similar trend among the three different arrangement

types. The pressure at the elevator door of the E-type arrangement (solid red line) reached a maximum positive value of 0.8 kPa for a wind direction of 60° and a maximum negative pressure of about -0.5 kPa for wind directions from 270° to 330° . Meanwhile, the pressure of the H-type arrangement (dotted blue line) reached a maximum positive value of 0.8 kPa at a wind direction of 30° and had the most negative pressure about -0.6 kPa. In terms of the pressure at the elevator door of the I-type arrangement (dotted green line), its variation for different wind directions is more similar to that of the H-type arrangement (dotted blue line) compared with that of the E-type (solid red line).

3. The Overall Wind Loads on Post-Installed Elevator Shafts

3.1. Wind Tunnel Tests

In order to obtain the overall wind loads on post-installed elevator shafts with E-type, H-type, and I-type arrangements (as shown in Figure 3) subjected to strong winds, high-frequency base balance wind tunnel tests with three installation arrangements and an individual elevator shaft (denoted as S-type) were carried out, as shown in Figure 3. These wind tunnel tests were conducted in the boundary-layer wind tunnel of Southwest Jiaotong University in China. The test section of the wind tunnel was 2.4 m in width and 2.0 m in height.

The scale model of the post-installed elevator shaft is 0.56 m in height, 0.058 m in width, and 0.048 m in length, as shown in Figure 3d. The B-type wind field is simulated according to China's load code for the design of building structures [46]. The wind profile and turbulence profile of a B-type wind field are shown in Figure 8. In Figure 8, α , which represents the exponent of power law for the vertical mean wind profile, is 0.15. I_u , U , and $U_{2/3H_T}$ are the turbulence intensity, wind speed, and wind speed at $2/3$ of H_T (gradient wind height), respectively. In these tests, 24 wind directions from 0° to 345° were considered, with intervals of 15° . The definition of wind direction is shown in Figure 9. When the wind direction β is 0° and 90° , the wind is blowing from the negative direction of the x-axis and the positive direction of the y-axis, respectively. The parameters of the wind tunnel tests are listed in Table 1. In Table 1, a wind speed of 10.2 m/s corresponds to the reference wind speed at a height of 90 cm in these wind tunnel tests.

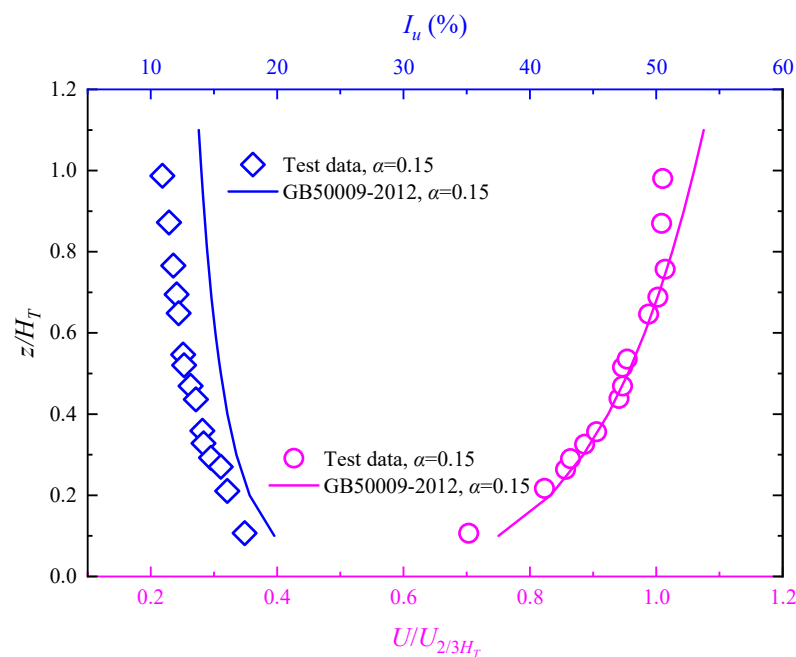


Figure 8. Profile of mean wind velocity and turbulence [46].

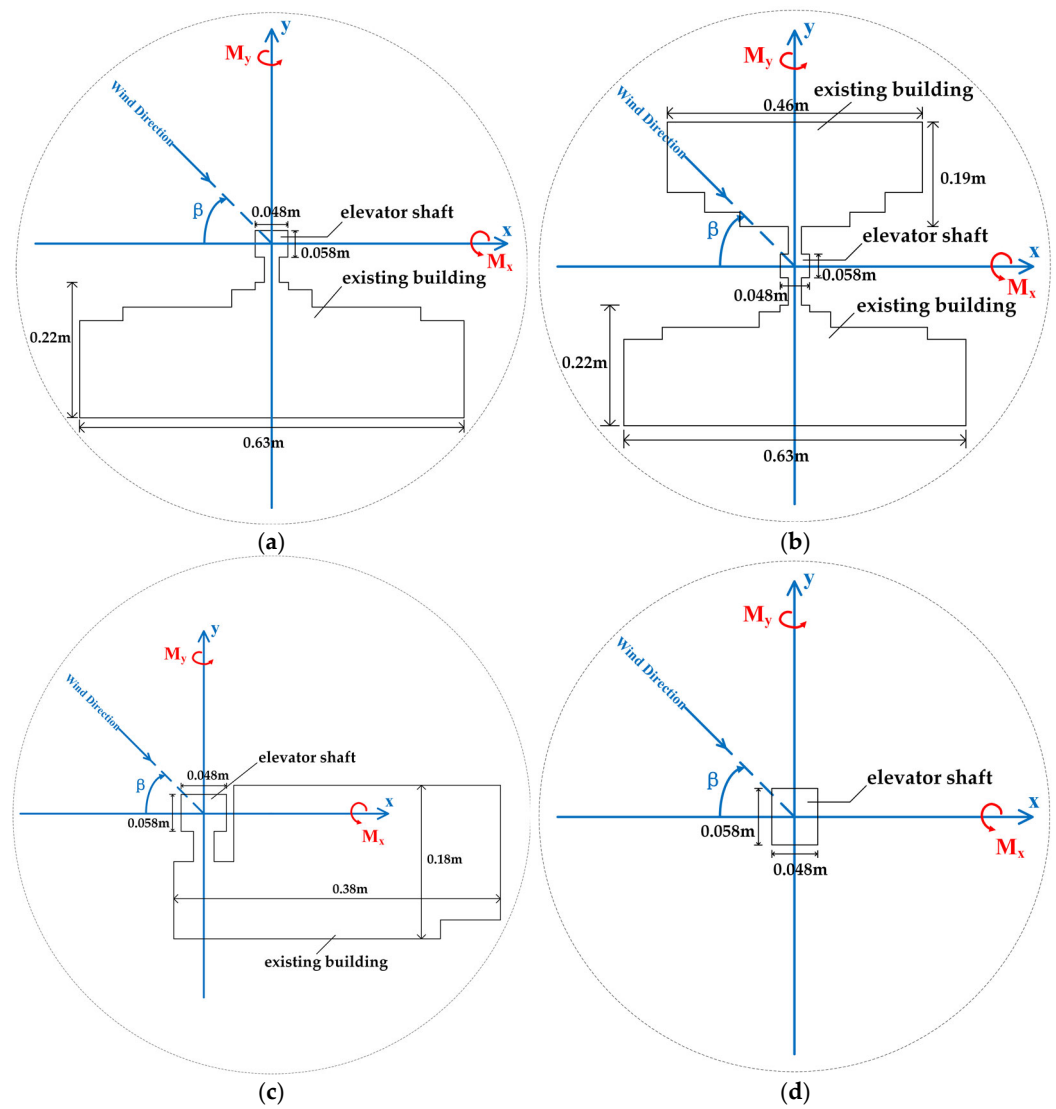


Figure 9. Definition of wind direction: (a) E-type, (b) H-type, (c) I-type, and (d) S-type arrangements.

Table 1. Wind tunnel test parameters.

Geometric Scale	Wind Speed	Sampling Frequency	Sampling Length	Incremental Step
1:50	10.2 m/s	300 HZ	5000	15°

3.2. Results of Overall Aerodynamic Coefficient of the Post-Installed Elevator Shafts

Based on the results from the wind tunnel tests with a high-frequency base balance, the overall shear forces and bending moments can be dimensionless; the dimensionless coefficient of overall aerodynamic forces $C_{F_i}(t)$ can be calculated as follows:

$$C_{F_i}(t) = \frac{F_i(t)}{\frac{1}{2}\rho v^2 B H} \quad (i = x, y) \quad (2)$$

$$C_{M_i}(t) = \frac{M_i(t)}{\frac{1}{2}\rho v^2 B H^2} \quad (i = x, y) \quad (3)$$

where $F_i(t)$, ρ , v , B and H represent the overall aerodynamic forces, air density, and reference wind speed of wind tunnel tests, and the width and the height of the tested model,

respectively. $M_i(t)$ represents the time history of aerodynamic bending moments. The average values of $C_{F_i}(t)$ and $C_{M_i}(t)$ can be written as \bar{C}_{F_i} and \bar{C}_{M_i} , respectively.

The time history of coefficients, which correspond to these overall aerodynamic forces on the elevator shafts with different arrangements and wind directions, are calculated according to Equations (2) and (3). Figure 10 presents the time history of the overall aerodynamic coefficients of elevator shafts with S-type arrangements (as shown in Figure 9d) under 90° and 180° wind directions. Figure 10 shows that the mean values of $C_{F_x}(t)$ and $C_{M_y}(t)$ in a 90° wind direction, as well as $C_{F_y}(t)$ and $C_{M_x}(t)$ in a 180° wind direction, reach zero due to the cross-wind aerodynamic forces under these wind directions.

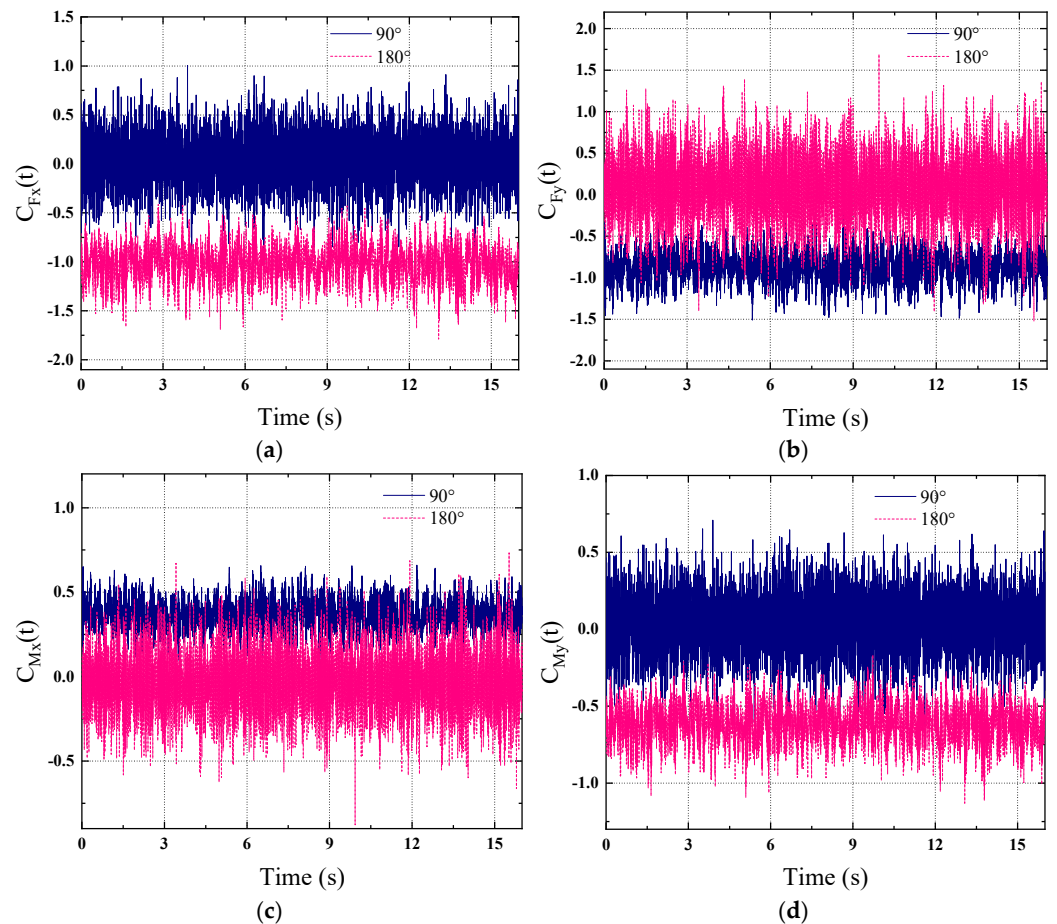


Figure 10. Time history of aerodynamic coefficients of the elevator shafts with S-type arrangements in 90° and 180° wind directions: (a) $C_{F_x}(t)$, (b) $C_{F_y}(t)$, (c) $C_{M_x}(t)$, and (d) $C_{M_y}(t)$.

Figures 11 and 12 present variations in \bar{C}_{F_x} and \bar{C}_{F_y} (the mean values of overall aerodynamic forces on the post-installed elevator shafts) with 24 wind directions, respectively. For an elevator shaft with an S-type arrangement (shown in Figure 11a as a red solid line), the values of \bar{C}_{F_x} have a symmetrical trend around a 180° wind direction, and the maximum negative (about -1.0) and positive values (about 1.0) occur for 180° and 0° wind directions, respectively. The values of \bar{C}_{F_x} corresponding to different arrangements (E-type, H-type, I-type, and S-type) are almost identical around the 0° – 30° wind directions, but the absolute value of \bar{C}_{F_x} for the post-installed elevator shaft with an I-type arrangement (dotted green line) has the lowest value among the four arrangement types for 180° – 270° wind directions. This is attributed to the aerodynamic interference effects of the existing building on the post-installed elevator shafts. In general, Figure 11a indicates that the effects of aerodynamic interference in existing buildings on post-installed elevator shafts are the most significant in the I-type arrangement for 24 wind directions. In Figure 11b, the values of \bar{C}_{F_y} show a dissymmetrical distribution for the 180° wind direction, and the aerodynamic interference

effects in the H-type arrangement (dotted blue line) are more significant than the other two arrangement types for $30^\circ \sim 150^\circ$ wind directions. However, the values of \bar{C}_{F_y} in the three arrangement types (E-type, H-type, and I-type) are almost same for wind directions between 195° and 300° due to the post-installed elevator shafts locating the wake flow of the existing buildings. Figure 12a,b present the variations in \bar{C}_{M_x} and \bar{C}_{M_y} with different wind directions. The variation trends for \bar{C}_{M_x} and \bar{C}_{M_y} corresponding to an elevator shaft with an S-type arrangement (red solid line in Figure 12a,b) with different wind directions is similar to the results for a single building in a previous study [47]. The values of \bar{C}_{M_x} and \bar{C}_{M_y} are relative to the values of \bar{C}_{F_y} and \bar{C}_{F_x} , respectively; therefore, the variation trends shown in Figure 12a,b are the same as those in Figure 11a,b.

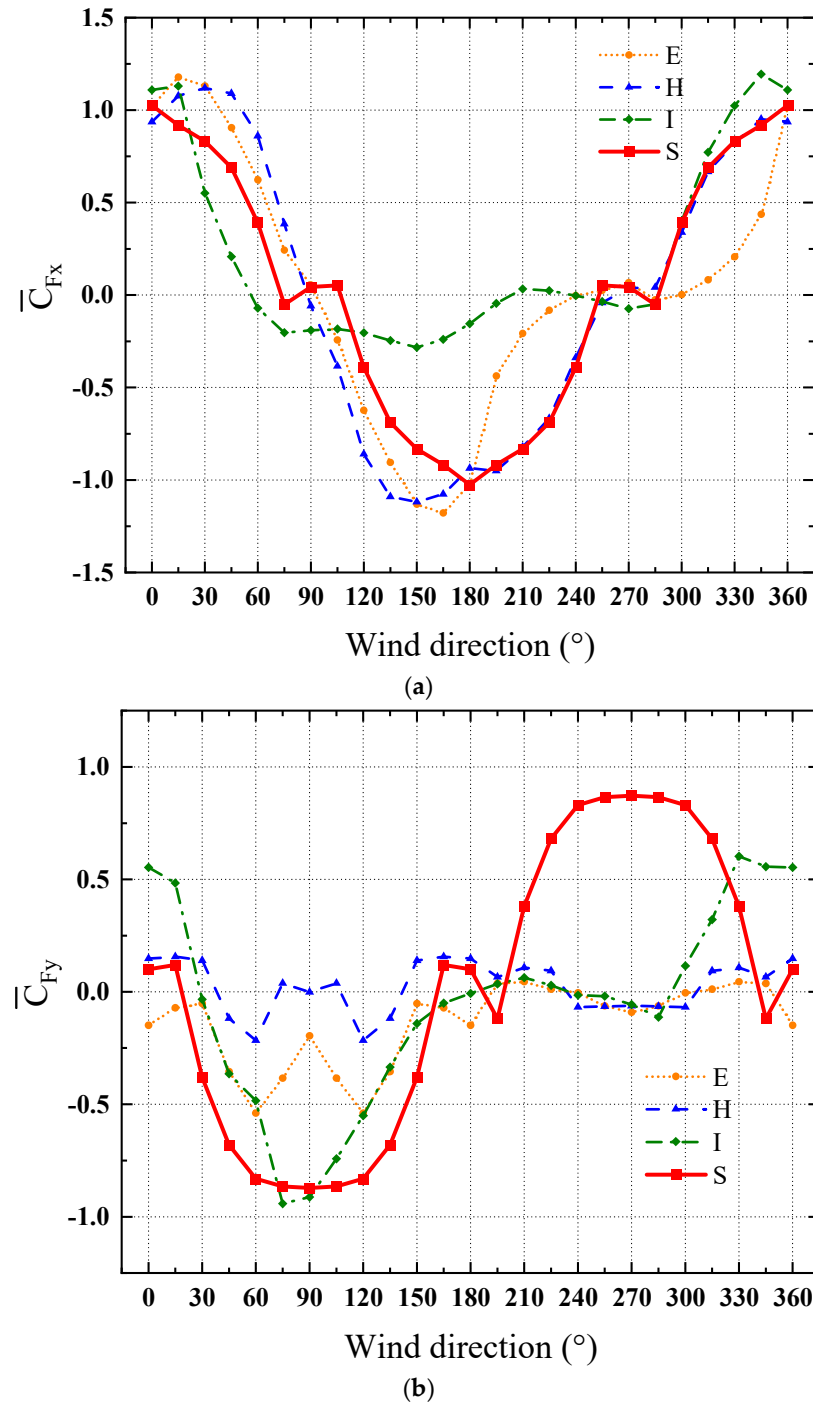


Figure 11. Variation in \bar{C}_{F_i} with different wind directions: (a) \bar{C}_{F_x} and (b) \bar{C}_{F_y} .

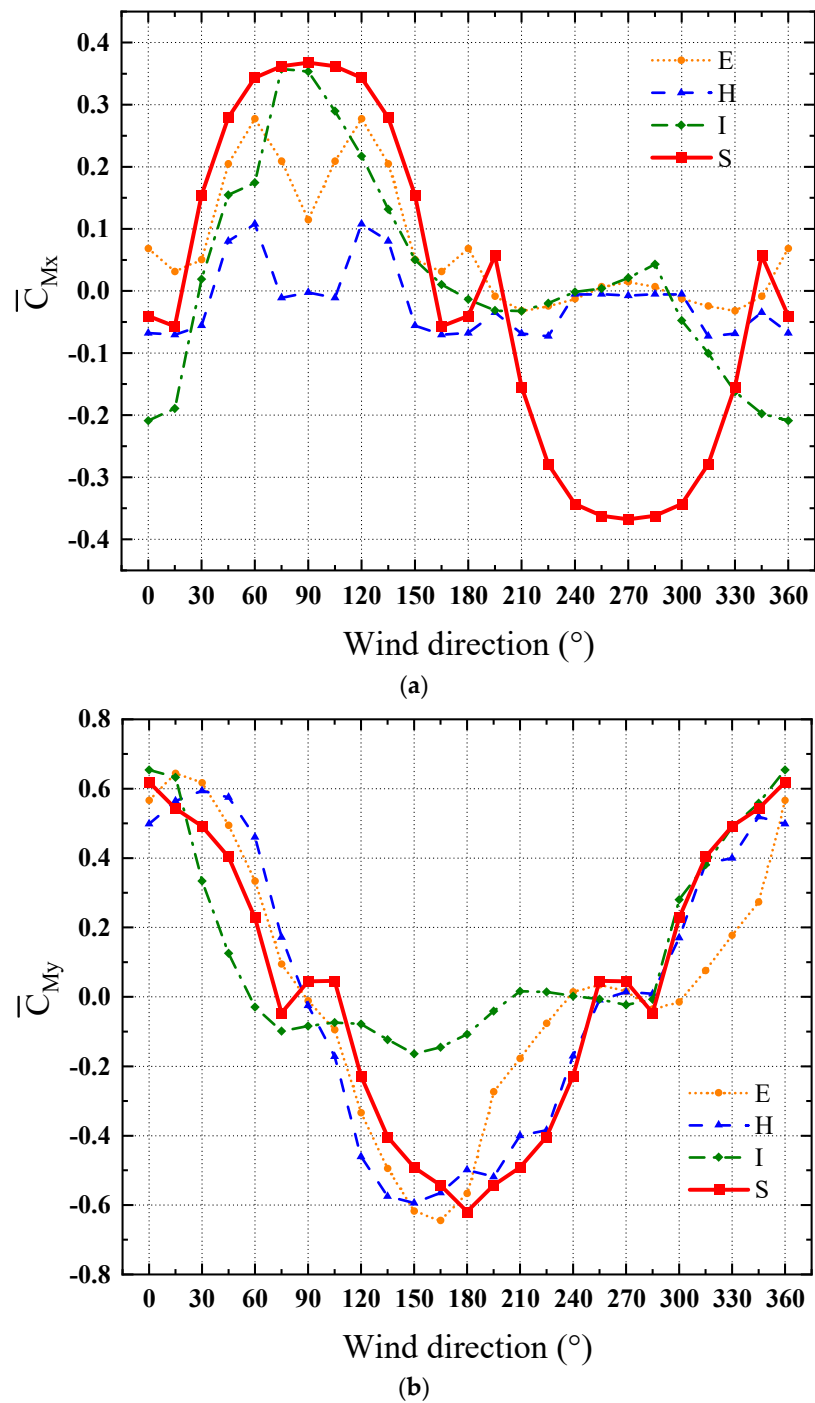


Figure 12. Variation in \bar{C}_{M_i} with different wind directions: (a) \bar{C}_{M_x} and (b) \bar{C}_{M_y} .

4. Wind-Induced Displacement Responses of Post-Installed Elevator Shafts

4.1. Background of Wind-Induced Responses Based on Wind Tunnel Tests

The equations of motion for multi-degree-of-freedom (MDOF) structures under wind excitations can be expressed as:

$$M\ddot{x}(t) + C\dot{x}(t) + Kx(t) = P(t) \tag{4}$$

where M , C , and K are the mass, damping, and stiffness matrix, respectively. $x(t)$, $\dot{x}(t)$, and $\ddot{x}(t)$ are the vectors of displacement, velocity, and acceleration responses, respectively.

For the wind-induced vibration of an elevator shaft, it is assumed that the responses are dominated by the first vibration mode, i.e., $x(t) \approx \varphi_1 q_1(t)$, where $q_1(t)$ and φ_1 are the

first-order generalized displacement and first vibration mode, respectively. By substituting $x(t) = \varphi_1 q_1(t)$ into Equation (4) and pre-multiplying Equation (4) by φ_1^T , where T denotes the transposition operation, the equation of motion of the first mode can be expressed as:

$$\ddot{q}_1(t) + 2\zeta_1\omega_1\dot{q}_1(t) + \omega_1^2 q_1(t) = \frac{p_1^*(t)}{m_1^*} \quad (5)$$

where m_1^* , ζ_1 , ω_1 , and $p_1^*(t)$ are the first-mode generalized mass, damping ratio, circular frequency, and generalized aerodynamic forces, respectively.

For high-frequency base balance wind tunnel tests of the elevator shaft, the $p_1^*(t)$ can be written as:

$$p_1^*(t) = \frac{M_{x\backslash y}(t)}{H} \quad (6)$$

where $M_{x\backslash y}(t)$ are bending moments along the X- or Y-axes induced by the aerodynamic forces on these elevator shafts. $M_{x\backslash y}(t)$ can be measured using high-frequency base balance wind tunnel tests. H is the height of the elevator shaft.

Furthermore, $q_1(t)$ can be obtained by solving Equation (5) using the Duhamel integral, and thus $x(t)$ can be obtained. Based on the obtained time histories of wind-induced displacement responses, the peak responses of displacement, \hat{D}_{dis} , can be estimated as follows:

$$\hat{D}_{\text{dis}} = \bar{D}_{\text{dis}} \pm g\sigma_{\text{dis}} \quad (7)$$

In Equation (7), \bar{D}_{dis} represents the average value of displacement response. g is the peak factor calculated based on Equation (8).

$$g = [2\ln(\eta T_w)]^{1/2} + \frac{0.577}{[2\ln(\eta T_w)]^{1/2}} \quad (8)$$

In Equation (8), T_w is the duration of the observation sample. η is the effective frequency of structural response, which can be conservatively considered as equal to the first natural frequency of the uncontrolled structure in Hz [48]. σ_{dis} represents the standard deviation of displacement responses.

4.2. Results of Wind-Induced Displacement Responses

Wind-induced displacement responses on the roof of post-installed elevator shafts are estimated according to overall aerodynamic forces and the dynamic characteristics of the elevator shaft at 24 wind directions. It is noted that the restraint of buildings to elevator shafts is neglected during an analysis of wind-induced displacement responses. Table 2 presents the first order of natural frequencies. Figure 13 presents a time history of wind-induced displacement responses of the elevator shafts with four arrangement types (as shown in Figure 9) along the X-axis for a 180° wind direction and along the Y-axis for a 90° wind direction.

Table 2. Structural dynamic characteristics.

Order	Frequencies (Hz)	Vibration Mode Direction	Damping Ratio
1	1.4	X-axis	0.02
2	1.6	Y-axis	0.02
3	2.1	Torsion	0.1

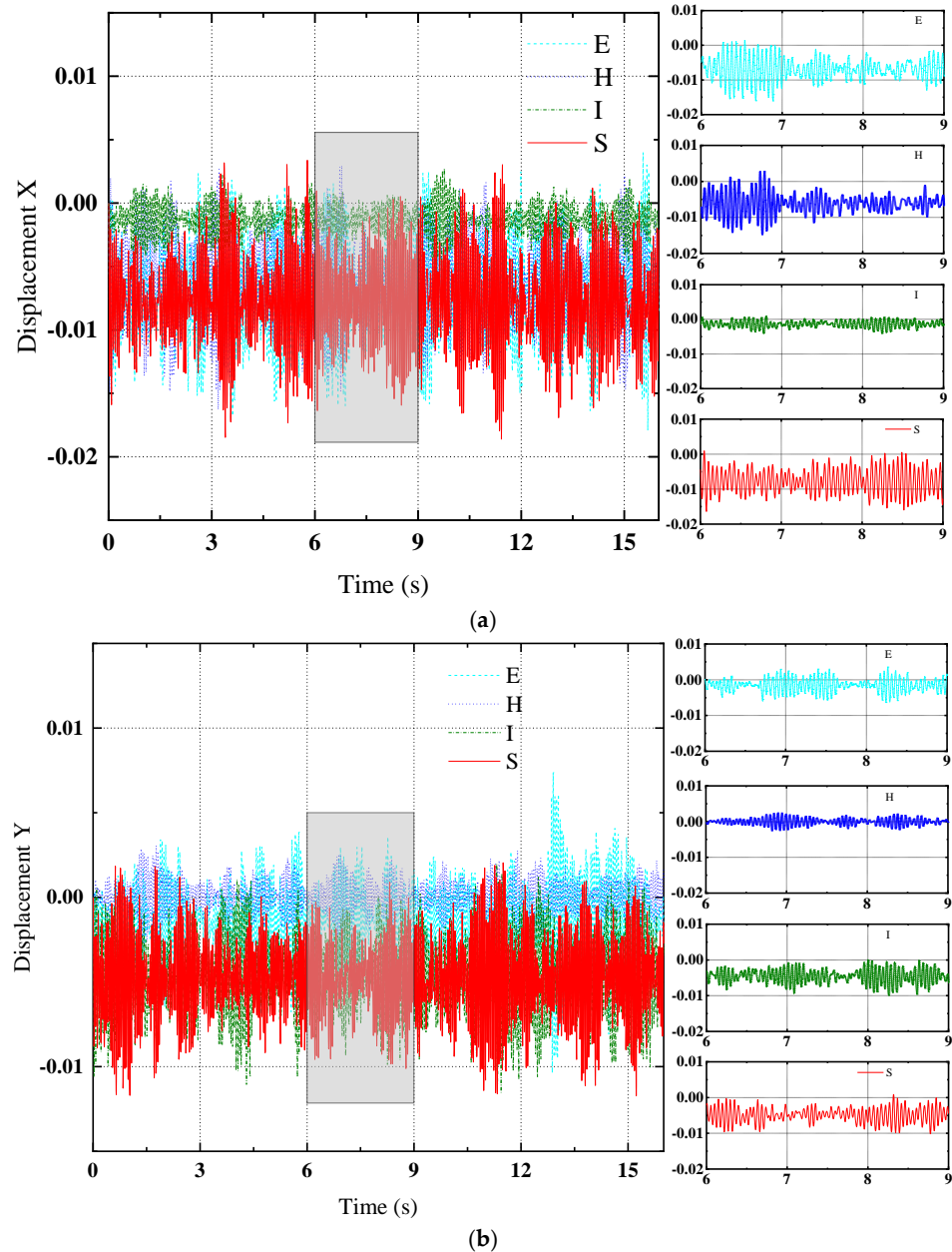


Figure 13. Time history of wind-induced displacement responses: (a) X-axis direction at 180° , (b) Y-axis direction at 90° .

The peak wind-induced displacement responses \hat{D}_{dis} under 24 wind directions were evaluated based on Equation (7). The variation in peak displacement responses along X-axis and Y-axis directions with different wind directions are shown in Figure 14a,b, respectively. Figure 14a demonstrates that the peak responses of the elevator shaft with an S-type arrangement (shown as a red solid line) from 0° to 180° are almost same as those observed from 360° to 180° due to the symmetrical character of the elevator shaft shape, and the absolute value of peak response along the X-axis reaches a maximum value of 0.02 m for 0° and 180° wind directions and a minimum value of 0.01 m for 90° and 270° wind directions. The effects of aerodynamic interference in existing buildings on post-installed shafts may affect the wind-induced peak displacement responses for the E-type, H-type, and I-type arrangements. For instance, the peak response of the E-type arrangement (dotted orange line in Figure 14a) is 0.022 for 30° and 150° wind directions, which is larger than that corresponding to the S-type arrangement; however, the absolute value of peak responses for the I-type arrangement (dotted green line in Figure 14a) is 0.005 in a 180° wind direction,

which is much lower than that in the S-type arrangement. In general, Figure 14a indicates that the aerodynamic interference in existing buildings most affected the wind-induced responses along the X-axis of the post-installed elevator shafts, especially in the I-type arrangement, at the wind directions from 120° to 240° . The maximum positive peak displacement is 0.028 m, which occurred in the I-type arrangement for a 15° wind direction. In Figure 14b, the peak responses of the Y-axis in terms of the S-type arrangement (shown as a red solid line) present a dissymmetrical distribution in the 180° wind direction and the maximum absolute value is 0.013 m, which occurs in wind directions between 90° and 270° . The effects of aerodynamic interference in existing buildings on the peak displacement responses of the elevator shaft with the H-type arrangement (dotted blue line in Figure 14b) are more significant than the other two types of arrangement (E-type and I-type), especially in the range of wind directions from 30° to 150° . Compared with the results for the S-type arrangement, the peak displacement of the post-installed elevator shafts with E-type and I-type arrangements (dotted orange and green line in Figure 14b, respectively) are negative in the range of wind directions from 240° to 270° due to the elevator shafts locating the wake flow of existing buildings. The peak displacement responses of the Y-axis are much lower than those along the X-axis.

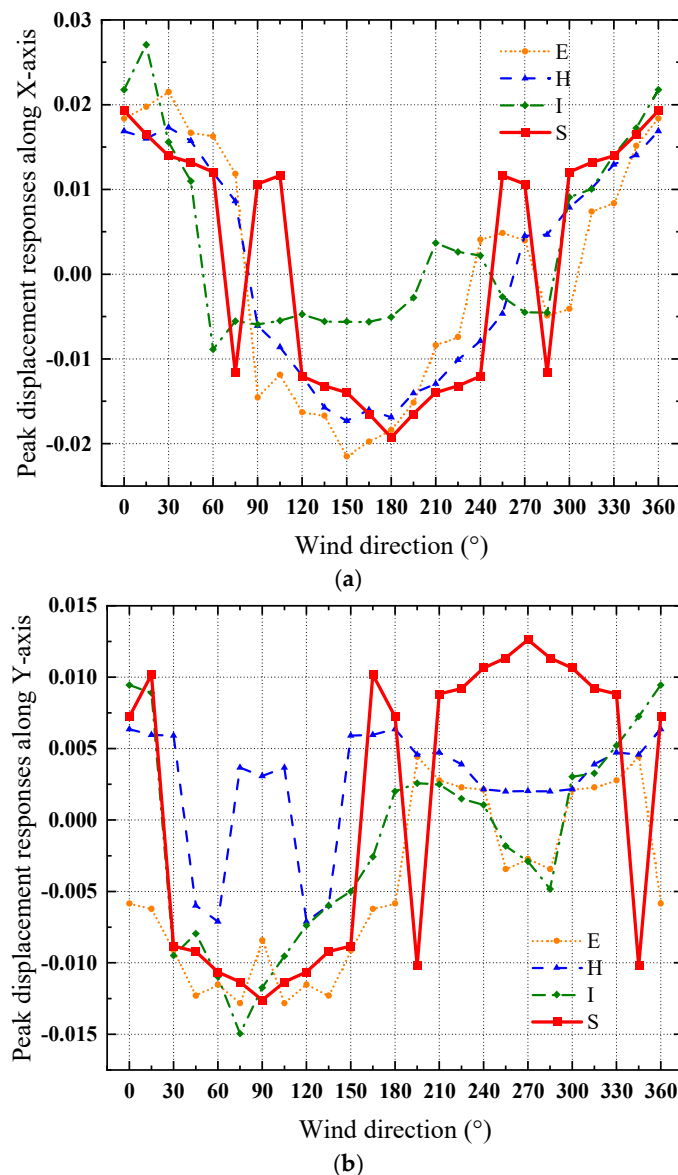


Figure 14. Peak displacement responses: (a) X-axis and (b) Y-axis.

5. Conclusions

To ensure that glass curtain walls are not damaged and that post-installed elevator shafts are serviceable under strong winds, the local and overall wind loads on post-installed elevator shafts (in three typical installation arrangements) were explored using CFD simulations and wind tunnel tests, and wind-induced displacement responses were further analyzed based on the results for the overall wind loads and dynamic characteristics of the elevator shafts. The main conclusions are as follows:

- (1) Among the three arrangement types of the post-installed elevator shaft, the maximum positive pressure coefficient on the elevator shaft surfaces is 1.14, observed in the I-type arrangement, and the maximum negative pressure coefficient on the elevator shaft surfaces is -1.43 , observed in the E-type arrangement. The wind pressure distribution of the elevator shaft surfaces with H-type arrangements is less affected by existing buildings than the other two arrangements. These results may provide engineers with a reference point for the wind-resistant design of envelopes (i.e., glass curtain walls) on post-installed elevator shafts.
- (2) The variation in local pressure on the door of the elevator shafts for certain wind directions shows a similar trend among the three different arrangement types (E-, H-type, and I-type arrangements). The maximum positive and negative local pressures on the area around the elevator shaft door are 0.8 and -0.6 kPa, respectively.
- (3) The effects of aerodynamic interference in existing buildings on the overall aerodynamic force coefficients \overline{C}_{F_x} of the post-installed elevator shafts are the most significant in the I-type arrangement among the three types of arrangements in 24 wind directions, while \overline{C}_{F_y} is the most affected by the aerodynamic interference in the H-type arrangement.
- (4) The aerodynamic interference in existing buildings also affects the peak wind-induced displacement responses of the post-installed elevator shafts, and the degree of effects varies with the wind direction. The maximum positive peak displacement along the X-axis is 0.028 m, which occurs in the I-type arrangement in a 15° wind direction, and the maximum negative displacement is -0.021 m, which occurs in the E-type arrangement in a 150° wind direction. The peak displacement responses along the Y-axis are less than those along the X-axis. These results might be helpful for the serviceability of designs for post-installed elevator shafts.

Author Contributions: H.Y.: conceptualization, methodology, software, and writing—original draft preparation. C.S.: funding acquisition, resources, methodology, supervision, formal analysis, and writing—review and editing. X.M.: conceptualization and data curation. J.S.: methodology and software, and data curation. All authors have read and agreed to the published version of the manuscript.

Funding: This research was funded by the Science and Technology Project of Huizhou City (grant number: 2020SC0206015).

Data Availability Statement: The data are available within the article.

Conflicts of Interest: The authors declare no conflicts of interest.

References

1. Huang, T. The Difficulties and Countermeasures of Installing Elevators in Existing Residential Buildings. In Proceedings of the 3rd International Conference on Culture, Education and Economic Development of Modern Society (ICCESE 2019), Moscow, Russia, 1–3 March 2019; Atlantis Press: Amsterdam, The Netherlands, 2019; pp. 1981–1985.
2. Chen, L.; Han, Q.X.; Tan, J.H. An Empirical Research on “Adding Elevators to Existing Residential Buildings”—Evidence from Guangzhou. In Proceedings of the 2nd International Workshop on Database Technology and Applications (DBTA), Wuhan, China, 27–28 November 2010.
3. Han, Q.X.; Ke, S.; Cui, X.L. Public Opinion Survey and Policy Suggestions on Adding Elevators to Old Buildings—Empirical Study from Guangzhou. *Adv. Mater. Res.* **2013**, *726–731*, 4954–4958. [[CrossRef](#)]
4. Guo, B.; Zhang, L.; Li, Y. Research on the path of residents’ willingness to upgrade by installing elevators in old residential quarters based on safety precautions. *Saf. Sci.* **2019**, *118*, 389–396. [[CrossRef](#)]

5. Gu, M.; Zou, J.; Li, H. Analysis on the Safety Status of Adding Elevators to Existing Residential Buildings in Zhenjiang and its Standardization Countermeasures. *China Stand.* **2018**, *A01*, 279–283.
6. Hitomi, N.; Morikawa, H.; Komiyama, S.; IEEE. Visualizing a Building's Structural Information from Inside an Elevator. In Proceedings of the 3rd IEEE Global Conference on Consumer Electronics (GCCE), Tokyo, Japan, 7–10 October 2014; pp. 588–592.
7. Ogawa, H. Actual conditions of elevators addition to the aged public housing in Japan and a proposal of an alternative method. In Proceedings of the 2005 World Sustainable Building Conference in Tokyo (CD-ROM), Tokyo, Japan, 27–29 September 2005.
8. Ogawa, H.; Fukao, S.; Yamazaki, S.; Kobayashi, K.; Kadowaki, K.; Minami, S.; Tahara, K. Development of a new elevator addition system for aged residential buildings-Development of the elevator tower system integrated with stairs Part 1. *AIJ J. Technol. Des.* **2007**, *13*, 715–720. [[CrossRef](#)]
9. Niedostatkiewicz, M.; Majewski, T.; Ziółkowski, P. Design errors of the external lift shaft and their negative impact on the operation of the clinic building. *MATEC Web Conf.* **2019**, *284*, 02006. [[CrossRef](#)]
10. Chen, Y.G.; Shen, L.M.; Wen, M.; Chen, B.K.; Jiang, J. Seismic Performance and Optimization Design of a Post-Installed Elevator Shear Wall Structure. *Buildings* **2023**, *13*, 18. [[CrossRef](#)]
11. Marinkovic, M.; Baballëku, M.; Isufi, B.; Blagojevic, N.; Milicevic, I.; Brzev, S. Performance of RC cast-in-place buildings during the November 26, 2019 Albania earthquake. *Bull. Earthq. Eng.* **2022**, *20*, 5427–5480. [[CrossRef](#)]
12. Foraboschi, P. Ultimate Shear Force of an Any Anchor Group Post-Installed into Concrete. *Materials* **2023**, *16*, 2608. [[CrossRef](#)]
13. Ruggieri, S.; Porco, F.; Uva, G. A numerical procedure for modeling the floor deformability in seismic analysis of existing RC buildings. *J. Build. Eng.* **2018**, *19*, 273–284. [[CrossRef](#)]
14. Zhou, L.N.; Ni, C.; Chui, Y.H.; Chen, Z.Y. Seismic Performance of a Hybrid Building System Consisting of a Light Wood Frame Structure and a Reinforced Masonry Core. *J. Perform. Constr. Facil.* **2014**, *28*, 8. [[CrossRef](#)]
15. Jiang, L.; Li, X.; Jiang, L.; Zhang, F.; Zheng, S. Shaking table tests on existing multi-story masonry residence with integrated technology of elevator retrofitting and seismic strengthening. *J. Build. Struct.* **2021**, *42*, 20–46.
16. Chen, B.; Jiang, L.; Zhang, L.; Yue, W.; Yang, H.; Yu, H. Wind Resistance Performance of Large-Scale Glass Curtain Walls Supported by a High-Rise Building. *Buildings* **2023**, *13*, 636. [[CrossRef](#)]
17. Gavanski, E.; Kopp, G.A. Glass Breakage Tests under Fluctuating Wind Loads. *J. Archit. Eng.* **2010**, *17*, 34–41. [[CrossRef](#)]
18. Yu, Y.; Liu, T.; Zhang, Q.; Yang, B. Wind-Induced Response of an L-Shaped Cable Support Glass Curtain Wall. *Shock. Vib.* **2017**, *2017*, 1–16. [[CrossRef](#)]
19. Dongmei, H.; Ledong, Z.; Quanshun, D.; Xue, Z.; Wei, C. Aeroelastic and aerodynamic interference effects on a high-rise building. *J. Fluids Struct.* **2017**, *69*, 355–381. [[CrossRef](#)]
20. Khanduri, A.C.; Stathopoulos, T.; Bédard, C. Wind-induced interference effects on buildings—A review of the state-of-the-art. *Eng. Struct.* **1998**, *20*, 617–630. [[CrossRef](#)]
21. Song, J.; Tse, K.T.; Tamura, Y.; Kareem, A. Aerodynamics of closely spaced buildings: With application to linked buildings. *J. Wind Eng. Ind. Aerodyn.* **2016**, *149*, 1–16. [[CrossRef](#)]
22. Sykes, D.M. Interference effects on the response of a tall building model. *J. Wind Eng. Ind. Aerodyn.* **1983**, *11*, 365–380. [[CrossRef](#)]
23. Yan, B.; Li, Q.S. Wind tunnel study of interference effects between twin super-tall buildings with aerodynamic modifications. *J. Wind Eng. Ind. Aerodyn. J. Int. Assoc. Wind Eng.* **2016**, *156*, 129–145. [[CrossRef](#)]
24. Boggs, D.W. The past, present and future of high-frequency balance testing. *Wind. Struct. An Int. J.* **2014**, *18*, 323–345. [[CrossRef](#)]
25. Rofail, A.W.; Holmes, J.D. High frequency base balance methodology for linked tall buildings. In Proceedings of the 12th International Conference on Wind Engineering, Cairns, QLD, Australia, 1–6 July 2007.
26. Tschanz, T.; Davenport, A.G. The base balance technique for the determination of dynamic wind loads. *J. Wind Eng. Ind. Aerodyn.* **1983**, *13*, 429–439. [[CrossRef](#)]
27. Zhang, L.; Wang, Y.; Xie, Z. Three-dimensional coupled wind-induced vibration calculation method for super high-rise buildings based on high-frequency force balance technology. *Struct. Des. Tall Spec. Build.* **2020**, *29*, e1772. [[CrossRef](#)]
28. Kim, Y.; You, K.P.; Ko, N.H. Across-wind responses of an aeroelastic tapered tall building. *J. Wind Eng. Ind. Aerodyn.* **2008**, *96*, 1307–1319. [[CrossRef](#)]
29. You, K.P.; Kim, Y.M.; Ko, N.H. The evaluation of wind-induced vibration responses to a tapered tall building. *Struct. Des. Tall Spec. Build.* **2008**, *17*, 655–667. [[CrossRef](#)]
30. Kim, Y.; Kanda, J. Characteristics of aerodynamic forces and pressures on square plan buildings with height variations. *J. Wind Eng. Ind. Aerodyn.* **2010**, *98*, 449–465. [[CrossRef](#)]
31. Mara, T.G.; Case, P.C. The Effects of Incremental Corner Modifications on a 200 m Tall Building. *ASCE* **2010**, *2010*, 2949–2960.
32. Tamura, Y.; Tanaka, H.; Ohtake, K.; Nakai, M.; Kim, Y. Aerodynamic Characteristics of Tall Building Models with Various Unconventional Configurations. In Proceedings of the Structures Congress, Orlando, FL, USA, 12–15 May 2010.
33. Bailey, P.A.; Kwok, K.C.S. Interference excitation of twin tall buildings. *J. Wind Eng. Ind. Aerodyn.* **1985**, *21*, 323–338. [[CrossRef](#)]
34. Kareem, A. The effect of aerodynamic interference on the dynamic response of prismatic structures. *J. Wind Eng. Ind. Aerodyn.* **1987**, *25*, 365–372. [[CrossRef](#)]
35. Xie, Z.N.; Gu, M. Mean interference effects among tall buildings. *Eng. Struct.* **2004**, *26*, 1173–1183. [[CrossRef](#)]
36. Gu, M.; Xie, Z.; Huang, P. Along-wind dynamic interference effects of tall buildings. *Adv. Struct. Eng.* **2005**, *8*, 623–636. [[CrossRef](#)]
37. Chen, B.; Shang, L.; Qin, M.; Chen, X.; Yang, Q. Wind interference effects of high-rise building on low-rise building with flat roof. *J. Wind Eng. Ind. Aerodyn.* **2018**, *183*, 88–113. [[CrossRef](#)]

38. Hui, Y.; Tamura, Y.; Yang, Q. Analysis of interference effects on torsional moment between two high-rise buildings based on pressure and flow field measurement. *J. Wind Eng. Ind. Aerodyn.* **2017**, *164*, 54–68. [[CrossRef](#)]
39. Kim, W.; Tamura, Y.; Yoshida, A. Interference effects on aerodynamic wind forces between two buildings. *J. Wind Eng. Ind. Aerodyn.* **2015**, *147*, 186–201. [[CrossRef](#)]
40. Sy, L.D.; Yamada, H.; Katsuchi, H. Interference effects of wind-over-top flow on high-rise buildings. *J. Wind Eng. Ind. Aerodyn.* **2019**, *187*, 85–96. [[CrossRef](#)]
41. Yu, X.; Xie, Z.; Gu, M. Interference effects between two tall buildings with different section sizes on wind-induced acceleration. *J. Wind Eng. Ind. Aerodyn.* **2018**, *182*, 16–26. [[CrossRef](#)]
42. Zhengwei, Z.; Yonga, Q.; Minga, G.; Nankuna, T.; Yongc, X. Effects of corner recession modification on aerodynamic coefficients of square tall buildings. In Proceedings of the 7th International Colloquium on Bluff Body Aerodynamics and Applications, Shanghai, China, 2–6 September 2012.
43. Yong, Q.; Ming, G.U. Power Spectra of Across-wind Loads on Super High-rise Buildings. *J. Tongji Univ.* **2002**, *30*, 627–632.
44. Tse, K.-T.; Hitchcock, P.A.; Kwok, K.C.; Thepmongkorn, S.; Chan, C.M. Economic perspectives of aerodynamic treatments of square tall buildings. *J. Wind. Eng. Ind. Aerodyn.* **2009**, *97*, 455–467. [[CrossRef](#)]
45. Available online: <http://news.cjn.cn/shxw/201509/t2703579.htm> (accessed on 8 December 2023). (In Chinese)
46. GB50009-2022; Load Code for the Design of Building Structures. China Architecture & Building Press: Beijing, China, 2022.
47. Ke, Y.; Shen, G.; Yu, H.; Xie, J. Effects of Corner Modification on the Wind-Induced Responses of High-Rise Buildings. *Appl. Sci.* **2022**, *12*, 9739. [[CrossRef](#)]
48. Davenport, A.G. Note on the Distribution of the Largest Value of a Random Function with Applications to Gust Loading. *Proc. Inst. Civ. Eng.* **1964**, *28*, 187–196. [[CrossRef](#)]

Disclaimer/Publisher’s Note: The statements, opinions and data contained in all publications are solely those of the individual author(s) and contributor(s) and not of MDPI and/or the editor(s). MDPI and/or the editor(s) disclaim responsibility for any injury to people or property resulting from any ideas, methods, instructions or products referred to in the content.